Biochimica et Biophysica Acta 1828 (2013) 1322–1328

Contents lists available at SciVerse ScienceDirect

Biochimica et Biophysica Acta

journal homepage: www.elsevier.com/locate/bbamem

Quantification of propidium iodide delivery using millisecond electric pulses: Experiments

Mohamed M. Sadik [a], Jianbo Li [a], Jerry W. Shan [a], David I. Shreiber [b], Hao Lin [a,*]

[a] Department of Mechanical and Aerospace Engineering, Rutgers, The State University of New Jersey, 98 Brett Road, Piscataway, NJ 08854, USA
[b] Department of Biomedical Engineering, Rutgers, The State University of New Jersey, 599 Taylor Road, Piscataway, NJ 08854, USA

ARTICLE INFO

Article history:
Received 24 May 2012
Received in revised form 21 November 2012
Accepted 3 January 2013
Available online 10 January 2013

Keywords:
Electroporation
Electrophoresis
Field Amplified sample stacking
Molecular delivery
Extracellular conductivity

ABSTRACT

The transport mechanisms in electroporation-mediated molecular delivery are experimentally investigated and quantified. In particular, the uptake of propidium iodide (PI) into single 3T3 fibroblasts is investigated with time- and space-resolved fluorescence microscopy, and as a function of extracellular buffer conductivity. During the pulse, both the peak and the total integrated fluorescence intensity exhibit an inverse correlation with extracellular conductivity. This behavior can be explained by an electrokinetic phenomenon known as Field-Amplified Sample Stacking (FASS). Furthermore, the respective contributions from electrophoresis and diffusion have been quantified; the former is shown to be consistently higher than the latter for the experimental conditions considered. The results are compared with a compact model to predict electrophoresis-mediated transport, and good agreement is found between the two. The combination of the experimental and modeling efforts provides an effective means for the quantitative diagnosis of electroporation.

1. Introduction

In the past three decades, electroporation-mediated molecular delivery has attracted significant attention due to its great potential for cell manipulation, both *in vivo* and *in vitro* [1–7]. In this technique, an applied electric field transiently permeabilizes the cell membrane and delivers biologically active molecules, such as DNA, RNA, proteins, or drug molecules into the cytoplasm, while maintaining cell viability and functionality [8–19]. This method of physical delivery is preferred in some applications over other delivery methods, such as chemical transfection and viral infection, due to its low cost, ease of operation, and promise for low toxicity [4,20,21].

Molecular delivery by electroporation is an intricate physical process involving two major aspects: (I) permeabilization of the membrane [22–24], and (II) transport of species into the permeabilized cell [14,15,26–28]. Research conducted over the past three decades has led to a relatively mature understanding of membrane permeabilization and well-developed theoretical models that describe this phenomenon [22,24,29]. Considerably less is known about the subsequent transport of species. Several mechanisms have been identified [1,5,6,8,14,15,23,27,28,30–36]. For instance, in DNA electrotransfer across the membrane, electrophoresis and membrane-DNA interactions, such as endocytosis, are involved [8,13,15,16,18,23,28,37,38]. Similarly, for smaller molecules such as propidium iodide (PI), calcium ions, and most drug molecules, which have molecular weights less than 4 kDa, simple diffusion and electrophoresis may influence the delivery [14,15,25,27,38–40]. Although each of these mechanisms can contribute to delivery, different findings exist on their relative importance [1,6,8,14,15,28,31,34,36,39–41]. For example, phototube measurements by Pucihar et al. revealed that free diffusion of PI post-pulsation contributed to most of the collected fluorescence signal, whereas a series of transdermal drug delivery experiments suggested that electrophoresis of charged molecules had the major contribution [13,14,35,42–46].

In this work, we aim to quantify the transport of small molecules using time- and space-resolved fluorescence microscopy. We investigate the delivery of PI into 3T3 mouse fibroblasts. The spatial evolution of the fluorescence profile is continuously monitored both during and after pulse application, and for six extracellular buffer electrical conductivities. Our work is motivated by the following considerations. First, we intend to quantify the respective contributions of electrophoresis and diffusion. In contrast to the phototube measurement by Pucihar et al., our experiments provide the necessary resolution to track the dynamic pattern of transport mechanism [14]. In addition, we explore a wider parametric range by varying the extracellular conductivity. Second, we aim to tackle the physical processes leading to the systematic behavior from earlier studies, namely the inverse correlation between delivery and extracellular conductivity observed by Zimmerman and co-authors [40,41]. However, in their work, the fluorescence signal for PI uptake was acquired by flow cytometry minutes after pulsation, and therefore did not reveal the spatial and the temporal dynamics of molecular entry. In the supra electroporation (nano-second pulse) study by Muller et al., only the result of the percentage of PI uptake was presented [40]. In addition, in [41], exponentially decaying pulses were used. Because the decay time is affected by and inversely correlated with the buffer conductivity, its effects on delivery could not be separated from those of other contributors [47]. Better

* Corresponding author. Tel.: +1 732 445 2322; fax: +1 732 445 3124.
E-mail address: hlin@jove.rutgers.edu (H. Lin).

0005-2736/$ – see front matter © 2013 Elsevier B.V. All rights reserved.
http://dx.doi.org/10.1016/j.bbamem.2013.01.002

controlled experiments are thus needed to help identify the root cause of the system behavior. Third, we aim to provide data to directly compare with model predictions. In recent model studies by two of us (JL and HL), we have discovered that Field-Amplified Sample Stacking (FASS), an electrokinetic mechanism arising from the presence of a non-uniform electric field, plays an important role in mediating molecular delivery via electrophoresis [48,49]. We proposed that this mechanism in part lead to the correlation observed in [40,41]. Furthermore, we have developed a simple formula to predict the total electrophoretic delivery, which is also a function of the extracellular conductivity. The current work will directly validate this model.

Our experiments are well controlled with pulses that are rectangular in shape, and not affected by the medium conductivity. For each experimental condition 30–50 single cell experiments were performed, and the results were averaged to achieve statistical significance. The analysis of the data reveals that during the pulse, both the peak and the total integrated fluorescence intensity exhibit an inverse correlation with extracellular conductivity. This behavior corroborates with the FASS theory proposed earlier [48,49]. In this case the non-uniformity of electric field is induced by the conductivity difference between the cytoplasm and the buffer [48]. A detailed account on the theory is found in [48]. Furthermore, the respective contributions from electrophoresis and diffusion have been quantified; the former is shown to be consistently higher than the latter for the experimental conditions considered. The results are compared with a compact model developed in [48,49] and good agreement is found between the two. In addition, we observe that cell swelling post-pulsation increases monotonically with the buffer conductivity, even though our buffers were isotonic in all cases.

2. Materials and methods

2.1. Cell culture

NIH 3T3 mouse fibroblasts were plated in six-well plates and cultured in Dulbecco's Modified Eagle Medium (DMEM) supplemented with Fetal Bovine Serum (FBS) (10% v/v), 1 penicillin–streptomycin (1% v/v), and L-glutamine (1% v/v) (Sigma, St. Louis, MO) at 37 °C and 5% CO_2. Cells were harvested at 70–80% confluency using 0.5% trypsin (Sigma) and washed once with DMEM prior to each experiment. For each experiment, 10–15 different cells were electroporated for each condition. All conditions were conducted on the same day from the same passage of cells, and the entire experimental design was repeated three times.

2.2. Reagents

The isosmotic pulsing buffers were prepared from 250 mM sucrose (Sigma), 10 mM HEPES (Sigma), and various concentrations of $MgCl_2$ salt (Sigma) (Table 1). The pH of the buffers was measured with a Beckman Φ 340 pH/Temp Meter (Beckman Coulter, Inc., Fullerton, CA) and was adjusted to 7.4. The osmolalities and conductivities of the solutions were measured with an Advanced Osmometer Model 3D3 (Advanced Instrument, Norwood, MA) and the CON 6/TDS 6 handheld Conductivity/TDS Meter (Oakton, Vernon Hills, IL), respectively. The osmolality of each solution was adjusted to 310 mOsm/kg by adding appropriate amounts of sucrose [50]. The values for the conductivity are presented in Table 1.

Table 1
List of experimental conditions. The extracellular buffer conductivity is denoted by σ_e.

Solution #	$MgCl_2$ (mM)	σ_e (μS/cm)	Total number of cells
1	0.4	100	42
2	1.1	250	35
3	2.4	500	34
4	3.8	750	41
5	5.2	1000	48
6	11.2	2000	43

2.3. Cell electroporation

After trypsinization for 5 min, cells were washed once with cell culture media to neutralize the trypsin and spun at 2000 rpm ($441\times g$) for 2 min (Allegra X-22 series, Beckman Coulter, Miami, FL). The supernatant was aspirated and the cell pellet was washed twice with the desired pulsing buffer, and spun both times at 500 rpm ($26\times g$) for 1 min. The final cell suspension was resuspended in 500 μL of pulsing buffer containing 100 μM of PI (668 Da) (Sigma). To perform electroporation experiments, approximately 30 μL of cells in suspension (10^4 cells/mL) was placed in a custom made electroporation chamber comprising two parallel stainless steel electrodes ($D = 0.61$ mm) affixed in 1 mm apart on a microscope slide. Calibrated, controlled square electric field pulses of 0.8 kV/cm strength and 100 ms pulse-width were applied utilizing a custom-built electroporator. We remark that this pulsing scheme would likely have resulted in significant cell death. However, the immediate purpose of this study is to understand the transport mechanisms during electroporation but not to optimize the process.

2.4. Fluorescence imaging

The electroporator was synchronized through a timing box (Model 535 Delay Generator, Berkeley Nucleonics, San Rafael, CA) with a CCD camera (ProgRes® JENOPTIK MF Cool, JENOPTEK Optical Systems, Inc., Jupiter, FL) attached to an inverted microscope (Olympus IX71, Center Valley, PA). The integrated system allowed image acquisition to begin before the onset of the electric pulse. Images were captured digitally at 40 frames-per-second (fps) for 7 s. The applied electric field was sufficient to permeabilize the cellular membrane and allowed entry of PI into the cell cytoplasm. Upon binding to DNA/RNA, PI emitted fluorescent signal (ex: 536 nm, em: 617 nm), which was quantified to measure the dynamic accumulation of the dye within the cell.

For reference, the maximum achievable fluorescence intensity was obtained from saponin treated cells. Cells were treated with 0.05% saponin (Sigma) and incubated on ice for 10 min. The cell suspension was washed twice with Phosphate Buffer Saline (PBS) without calcium and magnesium ions (Sigma) and incubated on ice for 20 min in PBS solution containing 100 μM of PI. The experiment was performed for a total of 20 cells. For each cell, a bright field image was taken to measure the cell size, and a single fluorescence image was acquired to measure the intensity.

2.5. Experimental analysis methods

All images and data were analyzed with MATLAB (The Mathworks, Inc., Natick, MA). To account for background fluorescence, the intensity from four 20 pixel × 20 pixel regions in the corners of each image, where continuous changes were never observed, was averaged and subtracted from the actual image. The fluorescence intensity profile along the cell centerline for each image was determined and averaged for all cells from the same condition. The total fluorescence intensity (TFI) inside a cell was calculated by integrating the signal over the whole projected cell area and normalized by either the initial cell volume or the final cell volume, since some changes in cell diameter were observed. As we will discuss in Section 4, a previously published model indicates that transport can depend on the cell size [49]. The normalization therefore, also serves to eliminate such effects such that the role of conductivity can be separated. The TFI was averaged over the total number of cells for each experimental condition listed in Table 1. The TFI for saponin treated cells was obtained similarly. The initial and final radii of each cell were determined from bright field images taken before the pulse and 30 s after the pulse ended, respectively.

3. Results

Representative images and centerline profiles of PI spreading in two buffers with different conductivities are shown in Fig. 1. The applied electric field was 0.8 kV/cm in strength, 100 ms in length, and pointed from left to right. Fig. 1A and B, shows the progression of the fluorescence signal inside the cell before the pulse ($t=-5$ ms), during the pulse (20 ms$<t<$95 ms), immediately after the pulse ($t=120$ ms), and well after the pulse ($t=5000$ ms). The cell periphery is indicated by white circles. PI initially entered the cell asymmetrically from the anode-facing side along the electric field during the pulse. After the pulse ceased, both spreading within the cell and PI entry from the cathode-facing side were observed. Fig. 1C and D, demonstrates the fluorescence intensity signal across the cell centerline. From the fluorescence images and the corresponding cell centerline plots, it is evident that the peak fluorescence intensity is higher for the low conductivity case ($\sigma_e=$ 100 μS/cm) than for the high conductivity case ($\sigma_e=2000$ μS/cm). The rate of increase of the peak fluorescence is greater during the pulse than after the pulse for both conductivities. The differences in the spatial and temporal evolution of fluorescence intensity during and after pulse application indicate that different mechanisms are involved in transporting PI during and post pulsation.

The dependence of the fluorescence intensity on the extracellular conductivity is more clearly demonstrated in Fig. 2. In Fig. 2A, the cell centerline profile at $t=95$ ms (the last frame before the end of the pulse) is shown for all six buffer conductivities. For each conductivity, the signal was obtained by averaging the centerline profile for all cells in that group. The fluorescence intensity consistently decreased with increasing buffer conductivity. The maximum value is plotted as a function of σ_e in Fig. 2B. The inverse correlation corroborates with findings from previous reports [40,41].

Fig. 3 examines electroporation-induced cell swelling. In Fig. 3A, the averaged cell radius both before and well after the pulse application is shown for the different buffer conditions. In Fig. 3B, the difference between the two is plotted. A monotonic increase in the degree of cell swelling as a function of buffer conductivity is observed. The measurement of the cell size is useful in normalizing the total fluorescence intensity, which is studied next.

Fig. 4 shows the evolution of the total fluorescence intensity (TFI) as a function of time and extracellular conductivity. The TFI is normalized by either the initial cell volume (Fig. 4A and B) or the final cell volume (Fig. 4C and D). The temporal evolution of the TFI for all six conductivities exhibits three distinguishable stages. The first stage occurs when the pulse is present (Fig. 4B and D). During this stage, the fluorescence signal increases sharply in a nearly linear fashion. The second stage starts after the pulse ceases and extends until approximately $t=1500$ ms (Fig. 4A and C). In this phase, the fluorescence continues to increase, but at a slower rate compared to that during the pulse, until it plateaus at around $t=1500$ ms. The last stage occurs from around $t=1500$ ms until the end of acquisition at $t=7000$ ms. During this period, the TFI remains nearly constant (Fig. 4A and C). In general, normalizing by the initial or final radii affected the magnitude of the TFI but not the trend of the results.

The contributions from the respective stages are illustrated in Fig. 5. The TFI for all cases was normalized by the average value derived from the 20 saponin treated cells (14,993 (a.u)), which provided a reference for the maximum achievable TFI when all binding sites are occupied. The curves with (■) describe the TFI values at the end of acquisition, which are accumulated from all three stages and represent total delivery. The curves with (▲) designate the TFI at the end of stage one, which represents the contribution from electrophoretic transport. The difference between the two is indicated by (●), which represents the contributions from post-pulsation transport, where diffusion is presumably the only available mechanism. The contribution from electrophoresis was consistently higher than that from diffusion for all cases. For comparison, the dashed lines are model predictions of electrophoresis mediated delivery from our earlier work [47,48]. The details of the formula and further discussion are found in the Discussion section.

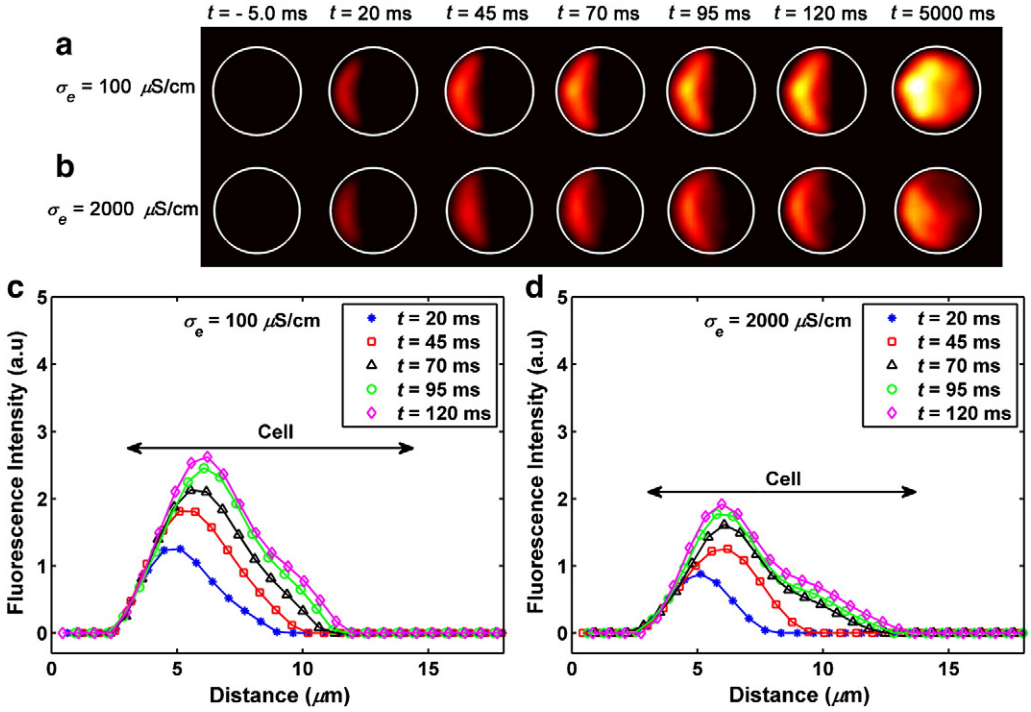

Fig. 1. Temporal dynamics of PI entry into electroporated 3T3 mouse fibroblasts. The applied electric field was 0.8 kV/cm in strength, 100 ms in length, and pointed from left to right. Typical progression of the fluorescence signal for two conductivities, (A) $\sigma_e=100$ μS/cm and (B) $\sigma_e=2000$ μS/cm, respectively. The fluorescence profile along the cell centerline for the cases shown in (A) and (B) are provided in (C) and (D), respectively. The fluorescence intensity for the low conductivity case is higher than that for the high conductivity case at all times.

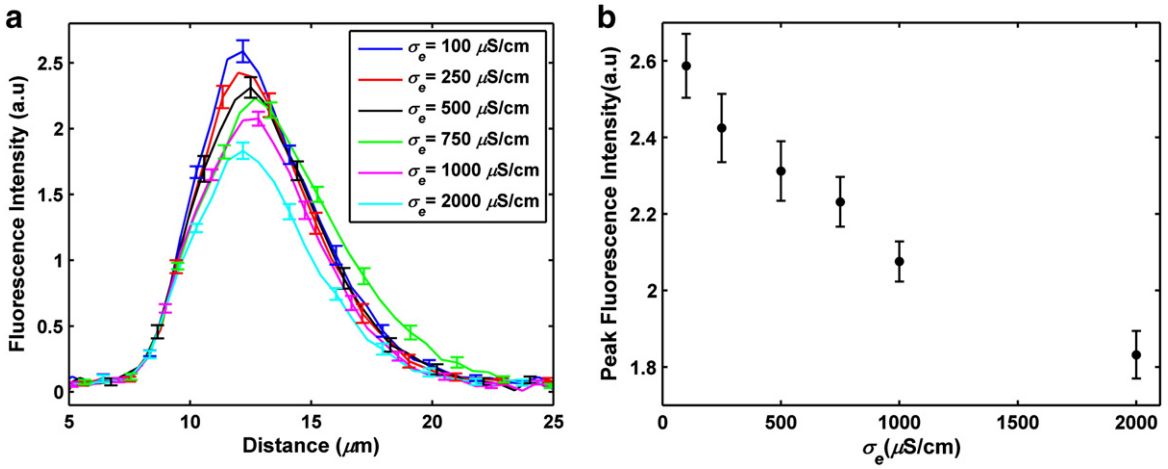

Fig. 2. (A) Average centerline fluorescence intensity profiles at $t = 95$ ms (the last frame acquired before the electric field was switched off) for the six buffer conductivities. (B) The peak intensity value is plotted as a function of buffer conductivity, which shows an inverse correlation between the two. Error bars represent standard error.

4. Discussion

The main objective of the current study is to analyze the mechanisms for molecular delivery via spatially and temporally resolved optical measurements. To this end, our results corroborate with the model prediction by two of us (JL and HL) that electrophoresis of the charged ions can be the dominant mode of transport [48,49].

In Figs. 1 and 2, our data show consistently that the peak fluorescence intensity, which indirectly indicates the peak PI concentration, is inversely correlated with the extracellular conductivity. We argue that this behavior is mediated by Field-Amplified Sample Stacking (FASS), which we proposed in [48]. Briefly, FASS is induced by the presence of a non-uniform electric field, which arises when a potential difference is applied across regions of different conductivities. The Ohmic equation dictates that the field strength is higher in the lower conductivity region (the extracellular buffer) compared to that in the higher conductivity region (the cytoplasm) ([48] Fig. 5B). This difference in field strength leads to different electrophoretic velocities in the two regions ([48] Fig. 5A). In particular, the ions slow down upon entering the cell cytoplasm, where the electrophoretic velocity is lower, causing "stacking" in that region. The ratio of concentration enhancement is given by Eq. (16) in [48], where the maximum ion concentration within the cell is inversely correlated with the extracellular conductivity, σ_e. This mechanism offers a viable interpretation of the trends observed in Figs. 1 and 2. However, one should note that the correlation in the experiments is not exactly reciprocal with respect to σ_e. This discrepancy may be attributed to the spatial convolution (in depth direction) of the signal emitted by the bound PI to determine peak fluorescence intensity, whereas the model prediction is for local free PI concentration in the absence of any binding reaction.

Fig. 5 further demonstrates the agreement between the experiment and the model prediction. The dashed lines represent calculations according to Eq. (12) in [49]:

$$c_{tot} = t_p c_e \omega F z E_o \pi a^2 \left(\frac{3\sigma_i}{2\sigma_e + \sigma_i}\right). \quad (1)$$

This equation is a compact formula to calculate the total molecules delivered into the cytoplasm (c_{tot}) via electrophoretic transport, and has been validated by full numerical simulations. In this equation t_p is the pulse length, c_e is the extracellular concentration of the target molecule, ω is the mobility of ions, F is Faraday's constant, z is the charge number, E_o is the field strength, a is the cell radius, and σ_i is the cytoplasm electrical conductivity. For the present calculation, $t_p =$ 100 ms, $c_e = 100$ μM, $\omega = 1.83 \times 10^{-13}$ m^2/(V.s), $F = 96{,}485$ C/mol, $E_o = 0.8$ kV/cm, $z = +2$, and $\sigma_i = 5000$ μS/cm. The extracellular conductivities, σ_e, are described in Table 1. The initial radii are used for the result in Fig. 5A, and the final radii are used in Fig. 5B. Finally, to compare with the experimental data, we normalized c_{tot} by 25 amoles, which is an estimate of the total binding sites within the cell according

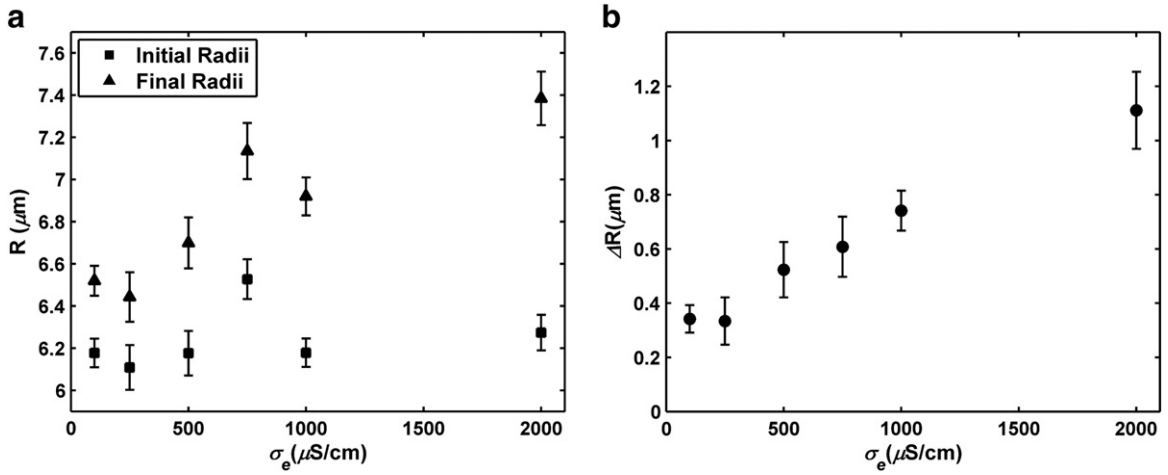

Fig. 3. (A) The average radius before (■) and after (▲) pulse application. (B) The increase in the average cell radius as a function of extracellular buffer conductivity. The cells swelled for each conductivity condition. Swelling increased monotonically with increasing buffer conductivity over the range studied. The error bars represent standard error.

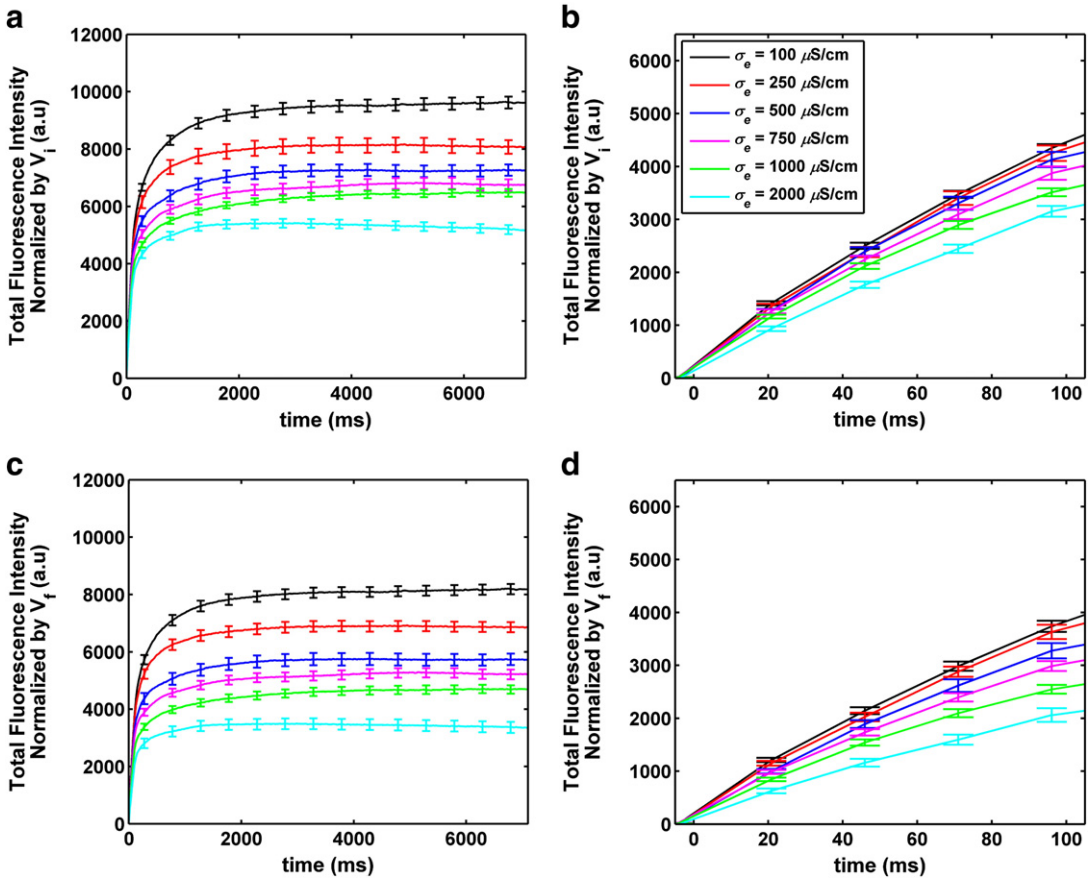

Fig. 4. The total fluorescence intensity (TFI) as a function of time and extracellular buffer conductivity. (A) and (B) The TFI is normalized by the initial cell volume. (C) and (D) The TFI is normalized by the final cell volume. The TFI rises sharply during the pulse (B and D). After the pulse ends, it continues to grow until plateauing at around 1500 ms (A and C). The error bars in the plots represent standard error. The TFI is inversely proportional to the extracellular conductivity for all cases.

to the measurements by Kennedy et al. (see Fig. 4 therein) [51]. When compared with the normalized TFI at $t = 95$ ms, closer agreement is found in Fig. 5A, whereas an over-prediction is observed in Fig. 5B. For both cases, the model captures the dependence of total delivery on the extracellular conductivity (the slope of the curves), which suggests that it provides a useful formula to estimate molecular delivery via electrophoresis. The results also suggest that the non-uniformity in the electrical field distribution plays a critical role in mediating molecular transport. Furthermore, because electrophoresis is the dominant mode of delivery in these cases, FASS related mechanisms also contribute significantly to the inverse correlation observed for total uptake.

After the pulse ceases at $t = 100$ ms, diffusion is presumably the only mechanism mediating transport. Its contribution is represented by the lowest curves in Fig. 5, where a peculiar inverse dependence on the extracellular conductivity is also observed. The cause of this dependence is unknown. In [49], the pore area density is predicted to have only a weak correlation with σ_e varying from 1000 μS/cm to 5000 μS/cm. Pucihar et al. demonstrated that the percentage of

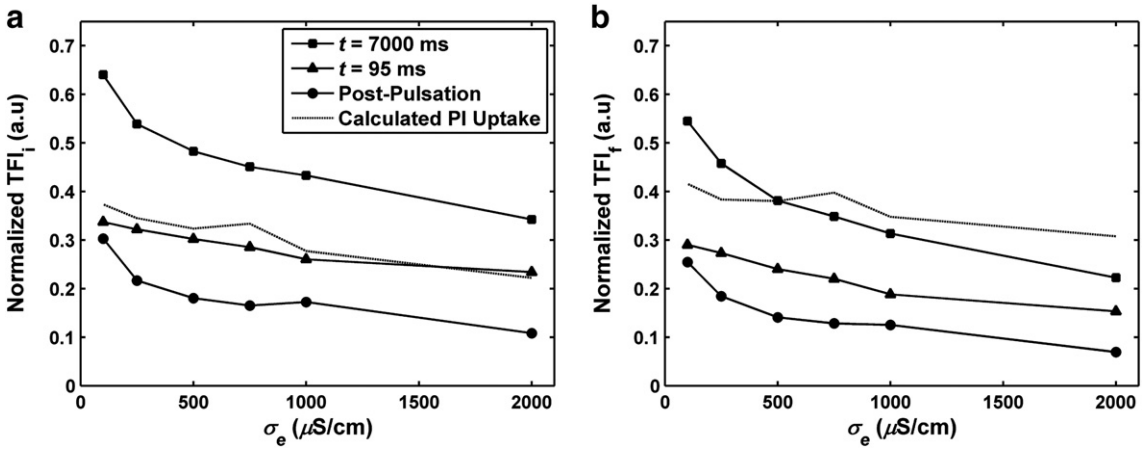

Fig. 5. (A) The total fluorescence intensity (TFI) extracted from Fig. 4A, and normalized by the maximum achievable TFI from saponin treated cells. (B) The TFI extracted from Fig. 4C, and normalized by the maximum achievable TFI from saponin treated cells. (■) Normalized TFI at the end of acquisition ($t = 7000$ ms). (▲) Normalized TFI close to the end of the pulse ($t = 95$ ms). (●) Difference between the TFI at the end of acquisition and the TFI at the end of the pulse. The dashed curves are theoretical predictions of electrophoresis mediated transport, calculated with the initial radii (A) and final radii (B), respectively.

permeabilized cells was not affected by the extracellular medium conductivity [52]. Furthermore, various authors even predicted consistently a positive correlation between membrane conductance, and permeabilization, with extracellular buffer conductivity [49,53], which is contrary to the dependence of delivery to the conductivity. More studies, following both experimental and modeling approaches, are needed to identify the underlying physical mechanisms behind the apparent decrease in post-pulsation diffusion with increasing buffer conductivity. On the other hand, we remark that the post-pulsation fluorescence might include contributions from the further binding of PI molecules already delivered into the cytoplasm during the pulse, as suggested in Fig. 4 in [48].

Finally, the present work has made an interesting discovery that swelling depends monotonically on the extracellular conductivity (Fig. 3). Note that all our solutions, regardless of the conductivity were isotonic. If the swelling is indeed controlled by the osmolarity of the cell, then the results suggest that more osmolarity enhancing molecules (e.g., Mg^{2+}, Cl^{-}, and sucrose) enter the cell at higher extracellular conductivities. We are currently performing modeling studies to correlate this data with a theoretical understanding.

5. Conclusion

In this work, we performed an extensive investigation on the transport mechanisms involved in electroporation-mediated molecular delivery. We used time- and space-resolved fluorescence microscopy to continuously monitor the uptake of PI into single 3T3 fibroblasts, and for six extracellular buffer electrical conductivities. During the pulse, both the peak intensity and the TFI exhibited an inverse correlation with extracellular conductivity. This behavior is explained by Field-Amplified Sample Stacking (FASS), which is an electrokinetic mechanism arising from the presence of a non-uniform electric field.

The respective contributions from electrophoresis and diffusion have been quantified. The former is shown to be consistently higher than the latter for the experimental conditions considered. Furthermore, the results are compared with a compact model to predict electrophoresis-mediated transport. Good agreement is found between the two, which validates the formula as a convenient tool to estimate molecular delivery via electrophoresis. It is hoped that the experimental quantification and modeling tools validated in this work will be important contributions toward designing optimized protocols for a wide range of applications utilizing electroporation.

Acknowledgements

M.M.S. gratefully acknowledges funding support from the IGERT program (NSF DGE 0801620). All authors acknowledge funding support from NSF (CBET 0967598 and CBET 0747886).

References

[1] F. Andre, L.M. Mir, DNA electrotransfer: its principles and an updated review of its therapeutic applications, Gene Ther. 11 (2004) S33–S42.
[2] M. Costa, M. Dottori, K. Sourris, P. Jamshidi, T. Hatzistavrou, R. Davis, L. Azzola, S. Jackson, S.M. Lim, M. Pera, A.G. Elefanty, E.G. Stanley, A method for genetic modification of human embryonic stem cells using electroporation, Nat. Protoc. 2 (2007) 792–796.
[3] J. Gehl, Electroporation: theory and methods, perspectives for drug delivery, gene therapy and research, Acta Physiol. Scand. 177 (2003) 437–447.
[4] J.C. Moore, K. Atze, P.L. Yeung, A.J. Toro-Ramos, C. Camarillo, K. Thompson, C.L. Ricupero, M.A. Brenneman, R.I. Cohen, R.P. Hart, Efficient, high-throughput transfection of human embryonic stem cells, Stem Cell Res. Ther. 1 (2010) 23.
[5] E. Neumann, M. Schaefer-Ridder, Y. Wang, P.H. Hofschneider, Gene transfer into mouse lyoma cells by electroporation in high electric fields, EMBO J. 1 (1982) 841–845.
[6] M.-P. Rols, J. Teissié, Electropermeabilization of mammalian cells to macromolecules: control by pulse duration, Biophys. J. 75 (1998) 1415–1423.
[7] J. Teissie, J.M. Escoffre, A. Paganin, S. Chabot, E. Bellard, L. Wasungu, M.P. Rols, M. Golzio, Drug delivery by electropulsation: recent developments in oncology, Int. J. Pharm. 423 (2012) 3–6.
[8] F. Andre, L.M. Mir, Nucleic acids electrotransfer in vivo: mechanisms and practical aspects, Curr. Gene Ther. 14 (2004) 267–280.
[9] J.C. Weaver, K.C. Smith, A.T. Esser, R.S. Son, T.R. Gowrishankar, A brief overview of electroporation pulse strength-duration space: a region where additional intracellular effects are expected, Bioelectrochemistry 87 (2012) 236–243.
[10] M. Kanduser, D. Miklavcic, M. Pavlin, Mechanisms involved in gene electrotransfer using high- and low-voltage pulses — an in vitro study, Bioelectrochemistry 74 (2009) 265–271.
[11] K. Kinosita Jr., I. Ashikawa, N. Saita, H. Yoshimura, H. Itoh, K. Nagayama, A. Ikegami, Electroporation of cell membrane visualized under a pulsed-laser fluorescence microscope, Biophys. J. 53 (1988) 1015–1019.
[12] Mojca Pavlin, Damijan Miklavcic, Theoretical and experimental analysis of conductivity, ion diffusion and molecular transport during cell electroporation - Relation between short-lived and long-lived pores, Bioelectrochemistry 74 (2008) 38–46.
[13] M.R. Prausnitz, J.D. Corbett, J.A. Gimm, D.E. Golan, R. Langer, J.C. Weaver, Millisecond measurement of transport during and after an electroporation pulse, Biophys. J. 68 (1995) 1864–1870.
[14] G. Pucihar, T. Kotnik, D. Miklavcic, J. Teissié, Kinetics of transmembrane transport of small molecules into electropermeabilized cells, Biophys. J. 95 (2008) 2837–2848.
[15] M.-P. Rols, J. Teissié, Electropermeabilization of mammalian cells to macromolecules: control by pulse duration, Biophys. J. 75 (1998) 1415–1423.
[16] S. Satkauskas, M.F. Bureau, M. Puc, A. Mahfoudi, D. Scherman, D. Miklavcic, L.M. Mir, Mechanisms of in vivo DNA electrotransfer: respective contributions of cell electropermeabilization and DNA electrophoresis, Mol. Ther. 5 (2002) 133–140.
[17] A. Silve, I. Leray, L.M. Mir, Demonstration of cell membrane permeabilization to medium-sized molecules caused by a single 10 ns electric pulse, Bioelectrochemistry 87 (2012) 260–264.
[18] J. Teissie, M. Golzio, M.P. Rols, Mechanisms of cell membrane electropermeabilization: a minireview of our present (lack of ?) knowledge, Biochim. Biophys. Acta (BBA) - Gen. Subj. 1724 (2005) 270–280.
[19] P.K. Wong, W. Tan, C.-M. Ho, Cell relaxation after electrodeformation: effect of latrunculin A on cytoskeletal actin, J. Biomech. 38 (2005) 529–535.
[20] L.M. Mir, Therapeutic perspectives of in vivo cell electropermeabilization, Bioelectrochemistry 53 (2001) 1–10.
[21] I. Richard, M. Ader, V. Sytnyk, A. Dityatev, G. Richard, M. Schachner, U. Bartsch, Electroporation-based gene transfer for efficient transfection of neural precursor cells, Brain Res. Mol. Brain Res. 138 (2005) 182–190.
[22] J.C. Neu, W. Krassowska, Asymptotic model of electroporation, Phys. Rev. E 59 (1999) 3471.
[23] K.C. Smith, J.C. Neu, W. Krassowska, Model of creation and evolution of stable electropores for DNA delivery, Biophys. J. 86 (2004) 2813–2826.
[24] J.C. Weaver, Y.A. Chizmadzhev, Theory of electroporation: a review, Bioelectrochem. Bioenerg. 41 (1996) 135–160.
[25] Kyle C. Smith, James C. Weaver, Transmembrane molecular transport during versus after extremely large, nanosecond electric pulses, Biochem. Biophys. Res. Commun. 412 (2011) 8–12.
[26] E. Neumann, S. Kakorin, I. Tsoneva, B. Nikolova, T. Tomov, Calcium-mediated DNA adsorption to yeast cells and kinetics of cell transformation by electroporation, Biophys. J. 71 (1996) 868–877.
[27] M. Pavlin, D. Miklavcic, Effective conductivity of a suspension of permeabilized cells: a theoretical analysis, Biophys. J. 85 (2003) 719–729.
[28] S.I. Sukharev, V.A. Klenchin, S.M. Serov, L.V. Chernomordik, A. Chizmadzhev Yu, Electroporation and electrophoretic DNA transfer into cells. The effect of DNA interaction with electropores, Biophys. J. 63 (1992) 1320–1327.
[29] W. Krassowska, P.D. Filev, Modeling electroporation in a single cell, Biophys. J. 92 (2007) 404–417.
[30] J.-M. Escoffre, T. Portet, L. Wasungu, J. Teissie, D. Dean, M.-P. Rols, What is (still not) known of the mechanism by which electroporation mediates gene transfer and expression in cells and tissues, Mol. Biotechnol. 41 (2009) 286–295.
[31] B. Gabriel, J. Teissie, Direct observation in the millisecond time range of fluorescent molecule asymmetrical interaction with the electropermeabilized cell membrane, Biophys. J. 73 (1997) 2630–2637.
[32] M. Yu, W. Tan, H. Lin, A stochastic model for DNA translocation through an electropore, BBA - Biomembranes 1818 (2012) 2494–2501.
[33] K.C. Smith, J.C. Neu, W. Krassowska, Model of creation and evolution of stable electropores for DNA delivery, Biophys. J. 86 (2004) 2813–2826.
[34] S.I. Sukharev, V.A. Klenchin, S.M. Serov, L.V. Chernomordik, A. Chizmadzhev Yu, Electroporation and electrophoretic DNA transfer into cells. The effect of DNA interaction with electropores, Biophys. J. 63 (1992) 1320–1327.
[35] D. Cukjati, D. Batiuskaite, F. André, D. Miklavcic, L.M. Mir, Real time electroporation control for accurate and safe in vivo non-viral gene therapy, Bioelectrochemistry 70 (2007) 501–507.
[36] M.F. Bureau, J. Gehl, V. Deleuze, L.M. Mir, D. Scherman, Importance of association between permeabilization and electrophoretic forces for intramuscular DNA electrotransfer, BBA-Gen. Subj. 1474 (2000) 353–359.
[37] J.-M. Escoffre, T. Portet, L. Wasungu, J. TeissiÃ©, D. Dean, M.-P. Rols, What is (still not) known of the mechanism by which electroporation mediates gene transfer and expression in cells and tissues, Mol. Biotechnol. 41 (2009) 286–295.
[38] M. Breton, L.M. Mir, Microsecond and nanosecond electric pulses in cancer treatments, Bioelectromagnetics 33 (2012) 106–123.
[39] B. Gabriel, J. Teissié, Time courses of mammalian cell electropermeabilization observed by millisecond imaging of membrane property changes during the pulse, Biophys. J. 76 (1999) 2158–2165.
[40] K.J. Muller, V.L. Sukhorukov, U. Zimmermann, Reversible electropermeabilization of mammalian cells by high-intensity, ultra-short pulses of submicrosecond duration, J. Membr. Biol. 184 (2001) 161–170.

[41] C.S. Djuzenova, U. Zimmermann, H. Frank, V.L. Sukhorukov, E. Richter, G. Fuhr, Effect of medium conductivity and composition on the uptake of propidium iodide into electropermeabilized myeloma cells, BBA-Biomembr. 1284 (1996) 143–152.
[42] A.-R. Denet, R. Vanbever, V. Preat, Skin electroporation for transdermal and topical delivery, Adv. Drug Deliv. Rev. 56 (2004) 659–674.
[43] M.R. Prausnitz, V.G. Bose, R. Langer, J.C. Weaver, Electroporation of mammalian skin: a mechanism to enhance transdermal drug delivery, Proc. Natl. Acad. Sci. U. S. A. 90 (1993) 10504–10508.
[44] R. Vanbever, E. LeBoulenge, V. Preat, Transdermal delivery of fentanyl by electroporation. I. Influence of electrical factors, Pharm. Res. 13 (1996) 559–565.
[45] R. Vanbever, N. Lecouturier, V. Preat, Transdermal delivery of metoprolol by electroporation, Pharm. Res. 11 (1994) 1657–1662.
[46] R. Vanbever, V. Preat, Transdermal drug delivery by skin electroporation in the rat, Methods Mol. Med. 37 (2000) 457–471.
[47] A. Ivorra, J. Villemejane, L.M. Mir, Electrical modeling of the influence of medium conductivity on electroporation, Phys. Chem. Chem. Phys. 12 (2010) 10055–10064.
[48] J. Li, H. Lin, Numerical simulation of molecular uptake via electroporation, Bioelectrochemistry 82 (2011) 10–21.
[49] J. Li, W. Tan, M. Yu, H. Lin, The effect of extracellular conductivity on electroporation-mediated molecular delivery, Biochimica et Biophysica Acta (BBA) – Biomembranes 1828 (2013) 461–470.
[50] M. Kanduser, D. Miklavcic, Electroporation in Biological Cell and Tissue: An Overview Electrotechnologies for Extraction from Food Plants and Biomaterials, Springer, New York, 2009, pp. 1–37.
[51] S.M. Kennedy, Z. Ji, J.C. Hedstrom, J.H. Booske, S.C. Hagness, Quantification of electroporative uptake kinetics and electric field heterogeneity effects in cells, Biophys. J. 94 (2008) 5018–5027.
[52] G. Pucihar, T. Kotnik, M. Kanduser, D. Miklavcic, The influence of medium conductivity on electropermeabilization and survival of cells in vitro, Bioelectrochemistry 54 (2001) 107–115.
[53] D.O.H. Suzuki, A. Ramos, M.C.M. Ribeiro, L.H. Cazarolli, F.R.M.B. Silva, L.D. Leite, J.L.B. Marques, Theoretical and experimental analysis of electroporated membrane conductance in cell suspension, IEEE Trans. Biomed. Eng. 58 (2011) 3310–3318.